

# Puzzle-AE: Novelty Detection in Images through Solving Puzzles

Mohammadreza Salehi  
 Sharif University of Technology  
 smrsalehi@ce.sharif.edu

Niousha Sadjadi\*  
 Sharif University of Technology  
 nsadjadi@ce.sharif.edu

Hamid R. Rabiee  
 Sharif University of Technology  
 rabiee@sharif.edu

Ainaz Eftekhar\*  
 Sharif University of Technology  
 aeftekhar@ce.sharif.edu

Mohammad Hossein Rohban  
 Sharif University of Technology  
 rohban@sharif.edu

## Abstract

*Autoencoder, as an essential part of many anomaly detection methods, is lacking flexibility on normal data in complex datasets. U-Net is proved to be effective for this purpose but overfits on the training data if trained by just using reconstruction error similar to other AE-based frameworks. Puzzle-solving, as a pretext task of self-supervised learning (SSL) methods, has earlier proved its ability in learning semantically meaningful features. We show that training U-Nets based on this task is an effective remedy that prevents overfitting and facilitates learning beyond pixel-level features. Shortcut solutions, however, are a big challenge in SSL tasks, including jigsaw puzzles. We propose adversarial robust training as an effective automatic shortcut removal. We achieve competitive or superior results compared to the State of the Art (SOTA) anomaly detection methods on various toy and real-world datasets. Unlike many competitors, the proposed framework is stable, fast, data-efficient, and does not require unprincipled early stopping.*

## 1. Introduction

Anomaly/novelty is defined as any digression from the essential features of any given phenomenon. The main task of novelty detection is to infer deviated features just from extracted normal training samples' features. For instance, having a model trained on healthy brain ct-scan images, it should be able to find non-healthy test input images by comparing current extracted features and the expected ones with different metrics [8, 9, 4].

Although *Area Under the Curve* (AUC) has been used

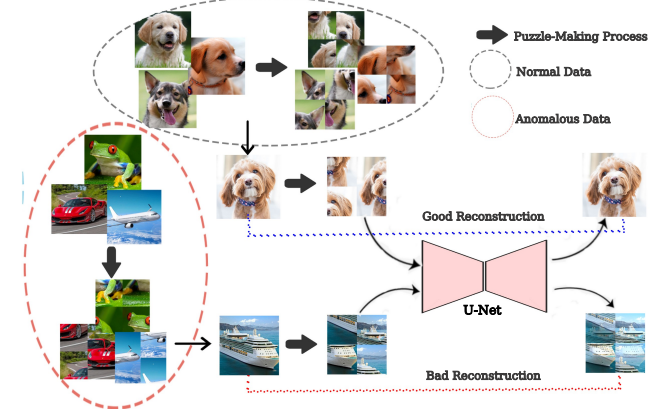


Figure 1: Reconstruction of normal and anomalous inputs during the testing phase. As it is shown, the model is unable to solve the puzzle for anomalous inputs, which do not have the main features existing in the normal data. As a result, anomalous samples produce high reconstruction loss, whereas normal inputs have low reconstruction loss since their puzzles are perfectly solved by the model.

as the main distinctive metric between binary classifiers' performances, this criterion is not sufficient alone. That is because AUC shows the average performance of a model in different operating points. However, a fixed operating point of the *Receiver Operating Characteristic* (ROC) curve is needed in many practical applications, which is usually when *True Positive Rate* (TPR) is equal to 0.99 or 0.995. In some applications such as medical and industrial defect detections, data efficiency and real-time performance are key factors for practicality [8, 14]. Another practical criterion is the adaptability of a given framework to other datasets. For

example, we generally require the model to be agnostic to the choices of various hyperparameters and also have access to well-known criteria to determine when to stop training of the model. In this paper, we propose a new framework and compare its practicality with the SOTA approaches with respect to the mentioned criteria. Our results show this framework performs well under all these criteria.

In the literature, GAN based methods [15],[24] suffer from non-reproducibility of the results [45],[31] and data hungriness. Likewise, autoregressive approaches have significantly poor performance [32]. Moreover, we show that one-class methods such as DSVDD [40] suffer from converging to trivial solutions and need confronting techniques such as early stopping that is not easy to find due to the one-class formulation of the problem. These all cause the generality and impracticality problem.

On the other hand, AE-based methods often have straightforward training process and yield reproducible results. It has been observed that an *Autoencoder* (AE) that is trained on just normal samples can reconstruct the normal test inputs while failing to reconstruct anomalous test samples [43]. However, various kinds of AEs have the issue of low-quality input reconstruction on complex datasets such as CIFAR-10 [25]. The reason for this phenomenon should be investigated in the training procedure of AE, which tries to model pixel intensities with a complex function that is represented by the decoder and leads to finding fallacious relationships between unnecessary or irrelevant features.

More recently, self-supervised learning methods have shown great potential to go beyond pixel-level and learn semantically meaningful features. Impressive unsupervised classification accuracy on the ImageNet [12] dataset in [52],[35],[56] has attracted a lot of attention to this field. GT [13] has introduced the first one-class classification method that utilizes self-supervised learning with great performance on the CIFAR-10 dataset [25]. However, we show that their performance is not even as good as the base AE on real-world datasets such as MVTecAD [5] and Medical images [23, 7].

We show that one way to benefit from all the great aspects of AEs and alleviate their deficiencies, is using U-Net [39] as a highly expressive AE-based model mixed with a well-defined and unambitious SSL pretext task. That is because U-Net has shown its ability in high-resolution image tasks such as segmentation [3, 29]. However, it could easily overfit when used similar to previous AE based methods such as denoising and etc. One great SSL pretext task that solves the overfitting problem and has the least effect on the data agnosticism of AEs, since it keeps almost all the input information, is puzzle-solving task [34, 18]. Training a U-Net to solve 4-part puzzled inputs like Fig. 1, would preserve good abilities of AEs while learning how to model normal input data in patch-level rather than pixel one.

However, according to [34], puzzles could be solved easily by finding low-level statistic shortcuts such as edge positions or patches' mean and variance. Instead of using traditional approaches such as manual jittering, adversarial robust training [30, 19] as an automatic shortcut removal is used to make the shortcuts out of access for the U-Net, which enhances semantical abstraction modeling. Finally, having trained the framework in a GAN-based setting by considering the U-Net as the generator and adding a discriminator, we could increase the quality of generated images even more [41].

Our framework shows great performance on large number of datasets. To the best of our knowledge, our work is the first study that produces a framework *without any need to design unprincipled early stopping criterion*, while producing stable and reproducible results. Our main contribution is to provide solutions for the following issues:

1. **High-quality normal sample reconstruction:** Significantly improving the AE flexibility to better reconstruct the normal samples in complex real-world datasets. This is achieved by learning beyond pixel-level abstraction using self-supervised training, removing some of the shortcut features by adversarial robust training, and improving the quality of generated images by training the whole framework similar to the *Generative Adversarial Network* (GAN).
2. **Method Stability:** The generative nature of our proposed self-supervised method helps in reaching a stable model across the training epochs. We empirically notice the lack of this property in the earlier self-supervised frameworks for the anomaly detection.
3. **Shortcuts in the Jigsaw:** Relieving the shortcut problem of the jigsaw puzzle pretext task (which is traditionally solved by manual jittering) automatically by adversarial robust training.
4. **Method Evaluation:** Introducing new practical criteria, *False Positive Rate* (FPR) at a high TPR, and robustness to the test-time adversarial attacks, that has not been tested on any recent SOTA models.
5. **Method Generality:** Competitive or better than SOTA performance on a *wide* range of problems without any need of unprincipled early stopping, and with a stable training process, yielding robust and reproducible results.

## 2. Related Works

The major approaches to the novelty detection are AE-based and one-class classification methods. Latent space autoregression (LSA) [1] is a popular AE-based method, which fits an autoregressive model to the AE bottleneck layer. By jointly training an autoregressive and AE model,

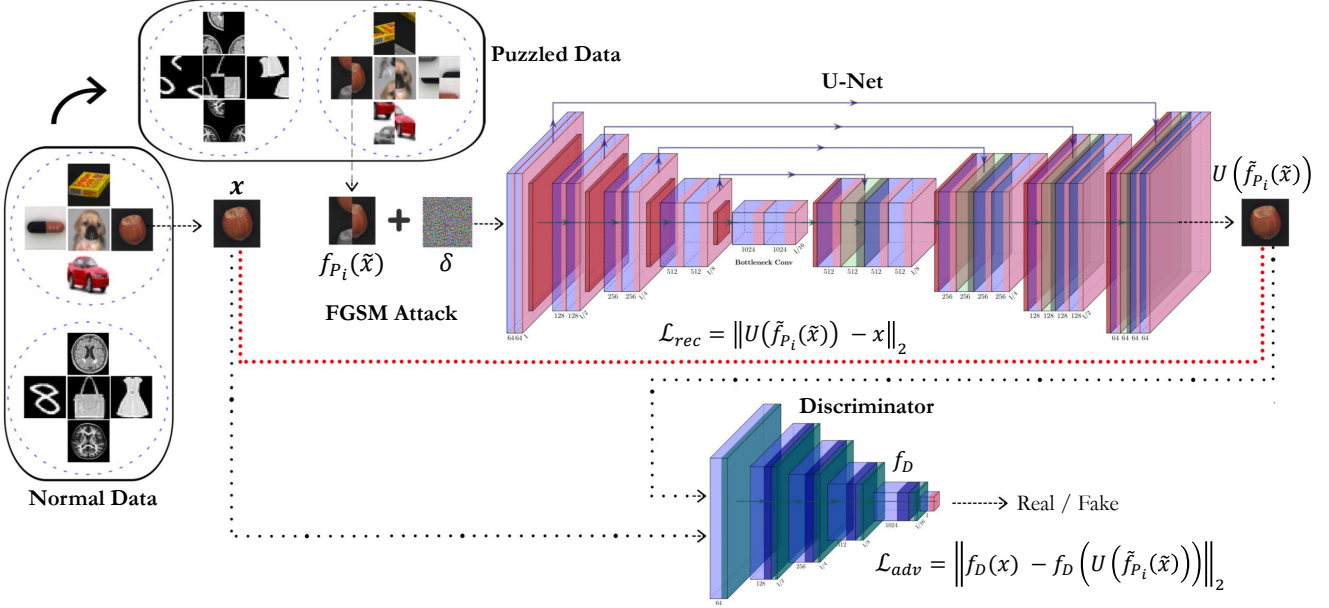


Figure 2: Anomaly Detection framework. As it illustrates, puzzled inputs are added to an FGSM noise to prevent shortcut detection. Then they are given to the U-Net to be solved. The whole framework is trained similar to GAN to improve the quality of reconstructed images.

it is able to learn a compact latent space for the normal samples. Hence, not only anomalous samples would have high reconstruction errors, but also the value of their bottleneck layer would have a lower probability than the normal ones. This probability is called “surprise score” in LSA. At testing time, the surprise score is added to the mean reconstruction error, and the sum is then thresholded to determine the class of a given sample.

OCGAN [36] uses an AE that is jointly trained with the reconstruction and generative adversarial error losses. In contrast to the LSA, it tries to force the encoder output distribution to be approximately uniform. This causes the decoder to reconstruct just normal outputs for both normal and anomalous inputs, which results in a higher mean squared error for abnormal input datum.

MemAE [14] is the first AE framework that uses memory in a non-parametric approach for novelty detection. When an input is passed to the AE, it is searched within the memory to find embeddings that match the input. Then, based on the combination of these embeddings, a new one is made and passed through the decoder.

Deep SVDD [40] is a one-class classification method that tries to convert data from the original space to a desired space by using deep neural networks. During the training process, it tries to put normal datum in a circle with a pre-defined center in a new space and then iteratively reduces its diameter. Because of the problem of finding trivial solutions, it uses early stopping and utilizes some constraints on the activation functions of layers. *Geometric Transforma-*

*tions* (GT) [13] is another one-class classification method that uses self-supervised learning. It makes a set of different transformations on the training data, and then by using a classifier, tries to guess which transformation is done on each input to ensure that in spite of anomalous inputs, normal ones are classified correctly at the testing time.

AnoGAN [46] is the first GAN based framework for novelty detection. It trains a GAN on the normal training datum. Then at the testing time, it looks for an appropriate latent vector such that the mean generator reconstruction error becomes lower than a certain threshold. Because of its high testing time, the authors in [2] introduced an improved version of AnoGAN, called Ganomaly, which does not need to solve any optimization problem at the testing time. Ganomaly employs *Variational Autoencoder* (VAE) [22] and GAN [16] frameworks to achieve its goal. Rather than solving the optimization problem at the testing time, it just uses the encoder part of VAE to obtain the desired latent vector.

### 3. Method

We propose the Puzzle-AE framework as a mixture of self-supervised learning methods and regular AEs in order to use the good features of both and reduce their important weaknesses.

### 3.1. Model Training

The proposed framework is illustrated schematically in Fig. 2. U-Net [27] architecture is used as our base framework that has a similar structure to AE but is popular because of its ability to reconstruct high-quality images, which is used by many segmentation methods [27, 29, 50]. However, we pass puzzled input rather than noisy or original image and it is expected from the U-Net [27] to reconstruct the right ordered image. The U-Net [27] is trained using the *Mean Square Error* (MSE) loss of its output and original input.

**Puzzle Making:** According to the principles of self-supervised learning, we use puzzle-solving as our pretext task. Each input image is split into 4 partitions and then a random permutation of these partitions with at least 2 displacements is selected. The 4-partition puzzle is chosen because it is the most evident way of making a puzzle, resulted in agnosticism about datasets. In order to obtain better features, puzzle-making procedure is combined with inpainting (for gray-scale images) or colorization (for colorful images). Thus, a partition is selected randomly to get fully black or grayscale accordingly.

Suppose we have a given input  $x \in \mathcal{X}$ , where  $\mathcal{X}$  denotes the entire training dataset. We first split this input into 4 partitions and convert a random partition to fully black or grayscale to obtain  $\tilde{x}$ . We show the set of puzzles as  $\mathcal{F} = \{f_{P_i}(\cdot) \mid i = 1, \dots, K\}$  where  $K$  is equal to 23 in case of having 4 partitions in each puzzle, and considering all the possible permutations of the partitions with at least 2 displacements.  $f_{P_i}(\tilde{x})$  denotes a specific permutation of the 4 partitions in which one partition is fully blacked or converted to black and white.

**Puzzle Making for Texture Images:** The defined set of puzzles  $\mathcal{F}$  determines the ambiguity of our self-supervised learning task. As mentioned in [34], a good self-supervised learning task should not be ambiguous. Now, considering texture-like images such as 5 texture categories in MVTecAD dataset, the 4 partitions in the puzzled image are mostly similar. Consequently, finding the right solution for all the 23 permutations of the partitions would be impossible. Therefore, to make our self-supervised learning task less ambiguous, only the 6 different permutations of the partitions with exactly 2 displacements are considered in our puzzle set  $\mathcal{F}$  which means  $K$  would be equal to 6 in this case.

**Adversarial Robust Training:** To avoid trivial or shortcut solutions in self-supervised learning methods such as finding low-level statistics of different partitions and finding partitions' border edges in the puzzled input. We obtain adversarial robust training as in [44] (that can be viewed as automatic shortcut removal) and also all of the inputs in both training and testing time have at least two displacements in their partitions. Since PGD [30] has a high time

complexity, we use FGSM [51], instead. Fig. 3 illustrates the aforementioned problem and the effect of adversarial robust training on solving it. As it is shown, FGSM [51] noise is added to the image purposefully to relieve the effect of low level statistics such as edges. Eq. 1 shows more details about the manipulation of FGSM [51] in the proposed framework.

$$\begin{cases} 1. \delta = Uniform(-\epsilon, \epsilon) \\ 2. \delta = \delta + \alpha \cdot \text{sign}(\nabla_x \|U(f_{P_i}(\tilde{x}) + \delta) - f_{P_i}(\tilde{x})\|_2) \\ 3. \delta = \max(\min(\delta, \epsilon), -\epsilon) \\ 4. \tilde{f}_{P_i}(\tilde{x}) = f_{P_i}(\tilde{x}) + \delta, \end{cases} \quad (1)$$

where  $U(\cdot)$  indicates the U-Net network,  $\epsilon$  is the attack magnitude, and  $\alpha$  is the step size.  $\tilde{f}_{P_i}(\tilde{x})$  is the adversarial sample obtained from the puzzled input  $f_{P_i}(\tilde{x})$ .

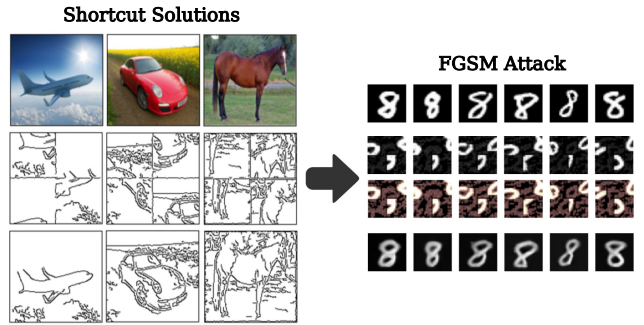


Figure 3: Some trivial features are produced that conduct the model to learn shortcuts. For example, model could understand the number of displacements just by noticing the vertical and horizontal lines. FGSM [51] makes specific anti-shortcut noises that appear similar to the number 8 (right figure). Heat map on the third row shows the normal image with better noise clarification.

**Adversarial Training and Total Loss:** The whole framework is also trained similar to the GAN framework [16] to improve the quality of the produced images. Better quality is obtained because of the ability of the adversarial training to converge to one mode in spite of MSE that converges to average of different modes [42, 9, 47]. We define the reconstruction loss  $\mathcal{L}_{rec}$  as the  $\mathcal{L}_2$  distance between the original input  $x$  which is drawn from the input data distribution  $p_x$ , and the solved puzzle at the output of the U-Net network  $U(\tilde{f}_{P_i}(\tilde{x}))$ :

$$\mathcal{L}_{rec} = \mathbb{E}_{x \sim p_x} \left\| U(\tilde{f}_{P_i}(\tilde{x})) - x \right\|_2. \quad (2)$$

Similar to [2], feature matching loss in the adversarial training is used.  $f_D(\cdot)$  denotes a function representing an intermediate layer of our discriminator  $D$ . The adversarial loss

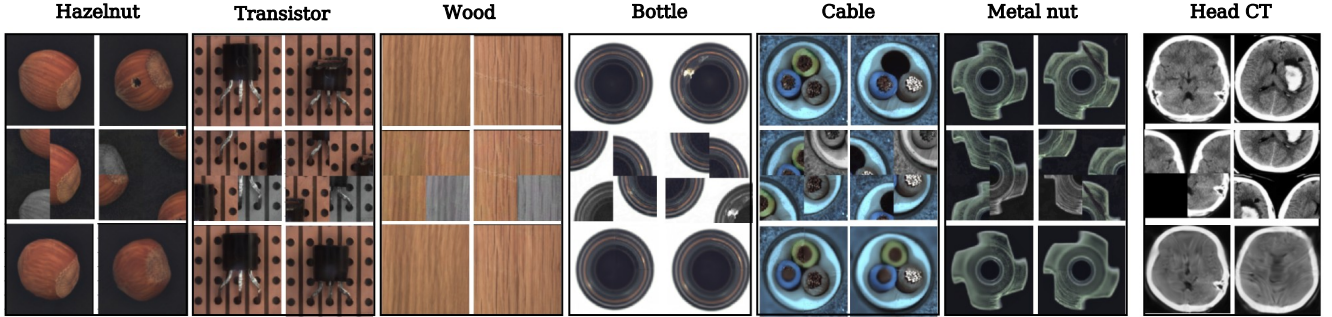


Figure 4: Visualization of the proposed method on MVTecAD [5] and Head CT datasets. First row is the original image, second row is the puzzled input mingled by colorization or inpainting and third row is the model’s output. For each category, first column is a normal input and the second column is an anomalous one.

$\mathcal{L}_{adv}$  is defined as follows:

$$\mathcal{L}_{adv} = \mathbb{E}_{x \sim p_x} \left\| f_D(x) - \mathbb{E}_{x \sim P_x} f_D \left( U \left( \tilde{f}_{P_i}(\tilde{x}) \right) \right) \right\|_2. \quad (3)$$

Finally, the total loss used as our total training objective is defined as:

$$\mathcal{L}_{total} = \mathcal{L}_{rec} + \lambda \mathcal{L}_{adv}, \quad (4)$$

where  $\lambda$  is a hyper-parameter defining the weight of the  $\mathcal{L}_{adv}$  term in the total loss.

### 3.2. Anomaly Score

The same puzzle-making procedure is used for evaluation. We split each test data into 4 partitions and consider all the  $K$  permutations of these partitions with at least 2 displacements without any inpainting or colorization auxiliary task. Suppose  $x$  is a given test data and the  $i^{\text{th}}$  permutation is used for the puzzle-making process to obtain  $f_{P_i}(x)$ . The anomaly score for this specific permutation is defined as:

$$\mathcal{S}_{test}^i = \|U(f_{P_i}(x)) - x\|_2. \quad (5)$$

**Error Normalization:** Since solving each of the  $K$  puzzles induce different difficulties for the model, the reconstruction error for some puzzles can be much larger than the others. Hence, different reconstruction errors can be obtained for a single input depending on the permutation used for the puzzle-making process. Therefore, we use validation data to normalize these errors over all the permutations. For this purpose, the average reconstruction error over all the validation data is computed for every single permutation. During test time, each reconstruction error is divided by the average error of validation data corresponding to that permutation :

$$\mathcal{S}_{test}^{i,i}(x) = \frac{\|U(f_{P_i}(x)) - x\|_2}{\mathbb{E}_{x \sim p_x} \|U(f_{P_i}(x)) - x\|_2}. \quad (6)$$

Finally, min, max and average anomaly score for all the  $K$  permutations of a single test data is computed:

$$\mathcal{S}_{test}(x) = \{\min \text{ OR } \max \text{ OR } avg\}_{1 \leq i \leq K} \{\mathcal{S}_{test}^{i,i}(x)\}. \quad (7)$$

The experiments show that using the max anomaly score is better for simple datasets, and as the dataset becomes more complex, using the average or min would yield better results. Therefore, to avoid unnecessary confusion and complexity in our performance measurement, we report the results by taking the max for the toy datasets and taking the average for the real-world datasets.

Fig. 4 shows the output of the model for some sample normal and anomalous inputs from MVTecAD [5] and Head CT (hemorrhage) dataset. See appendix for more sample images from different datasets.

## 4. Experiments

In this section, we validate our method by conducting extensive experiments. We consider multiple commonly used toy and also real-world datasets for evaluating our model. <sup>1</sup>

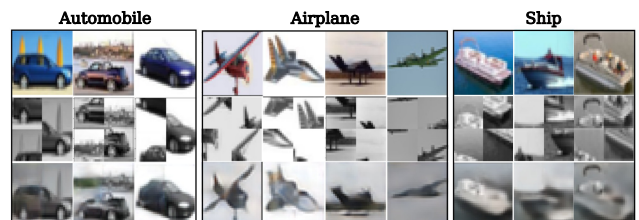


Figure 5: Effect of converting images to grayscale on the model learned features for some classes of CIFAR-10 [25] dataset. As it is shown, the model can produce perfect outputs even for grayscale inputs.

<sup>1</sup>Code to reproduce the results is provided at [https://github.com/Niousha12/Puzzle\\_Anomaly\\_Detection](https://github.com/Niousha12/Puzzle_Anomaly_Detection).

Table 1: AUROC in % for several datasets. As it is shown, Puzzle-AE surpass the SOTA by 7% on average on the CIFAR-10 [25] dataset while it is still competitive on the other ones.

Dataset	Method	0	1	2	3	4	5	6	7	8	9	Mean
MNIST [26]	RAAE [44]	99.8	99.9	96.0	97.2	97.0	97.4	99.5	96.9	92.4	98.5	97.5
	OCSVM [11]	99.5	99.9	92.6	93.6	96.7	95.5	98.7	96.6	90.3	96.2	96.0
	AnoGAN [46]	96.6	99.2	85.0	88.7	89.4	88.3	94.7	93.5	84.9	92.4	91.3
	DSVDD [40]	98.0	99.7	91.7	91.9	94.9	88.5	98.3	94.6	93.9	96.5	94.8
	CapsNetpp [28]	99.8	99.0	98.4	97.6	93.5	97.0	94.2	98.7	99.3	99.0	97.7
	OCGAN [36]	99.8	99.9	94.2	96.3	97.5	98.0	99.1	98.1	93.9	98.1	97.5
	LSA [1]	99.3	99.9	95.9	96.6	95.6	96.4	99.4	98.0	95.3	98.1	97.5
OURS		99.6 $\pm$ 0.004	99.93 $\pm$ 0.004	97.12 $\pm$ 0.083	96.97 $\pm$ 0.039	97.70 $\pm$ 0.017	98.43 $\pm$ 0.022	99.29 $\pm$ 0.041	98.26 $\pm$ 0.036	94.14 $\pm$ 0.073	98.57 $\pm$ 0.082	<b>98.00</b>
Fashion-MNIST [53]	RAAE [44]	93.7	99.1	91.1	94.4	92.3	91.4	83.6	98.9	93.9	97.9	<b>93.6</b>
	OCSVM [11]	91.9	99.0	89.4	94.2	90.7	91.8	83.4	98.8	90.3	98.2	92.8
	DAGMM [57]	30.3	31.1	47.5	48.1	49.9	41.3	42.0	37.4	51.8	37.8	41.7
	DSEBM [55]	89.1	56.0	86.1	90.3	88.4	85.9	78.2	98.1	86.5	96.7	85.5
	DSVDD [40]	98.2	90.3	90.7	94.2	89.4	91.8	83.4	98.8	91.9	99.0	92.8
	LSA [1]	91.6	98.3	87.8	92.3	89.7	90.7	84.1	97.7	91.0	98.4	92.2
	OURS(4-parts)	91.37 $\pm$ 0.200	98.96 $\pm$ 0.019	89.34 $\pm$ 0.056	92.04 $\pm$ 0.317	91.04 $\pm$ 0.087	90.73 $\pm$ 0.189	82.39 $\pm$ 0.077	98.23 $\pm$ 0.026	91.02 $\pm$ 0.190	97.52 $\pm$ 0.200	92.26
OURS(9-parts) <sup>2</sup>		91.73 $\pm$ 0.621	98.74 $\pm$ 0.133	89.92 $\pm$ 0.252	91.94 $\pm$ 0.612	89.69 $\pm$ 0.566	93.54 $\pm$ 0.606	84.90 $\pm$ 0.405	98.78 $\pm$ 0.078	92.30 $\pm$ 1.178	98.46 $\pm$ 0.169	93.00
CIFAR-10 [25]	RAAE [44]	72.2	43.1	69.0	55.0	75.2	54.7	70.1	51.0	72.2	40.0	60.23
	OCSVM [11]	63.0	44.0	64.9	48.7	73.5	50.0	72.5	53.3	64.9	50.8	58.56
	AnoGAN [46]	67.1	54.7	52.9	54.5	65.1	60.3	58.5	62.5	75.8	66.5	61.79
	DSVDD [40]	61.7	65.9	50.8	59.1	60.9	65.7	67.7	67.3	75.9	73.1	64.81
	CapsNetpp [28]	62.2	45.5	67.1	67.5	68.3	63.5	72.7	67.3	71.0	46.6	61.2
	OCGAN [36]	75.7	53.1	64.0	62.0	72.3	62.0	72.3	57.5	82.0	55.4	65.66
	LSA [1]	73.5	58.0	69.0	54.2	76.1	54.6	75.1	53.5	71.7	54.8	64.1
OURS		78.93 $\pm$ 0.203	78.05 $\pm$ 0.755	69.95 $\pm$ 0.344	54.88 $\pm$ 0.410	75.46 $\pm$ 0.204	66.04 $\pm$ 0.430	74.76 $\pm$ 0.280	73.30 $\pm$ 0.468	83.34 $\pm$ 0.256	69.96 $\pm$ 0.461	<b>72.47</b>

Table 2: AUROC in % on MVTec AD [5] dataset. We surpass the SOTA by  $\sim 4.6\%$ .

Method	Bottle	Hazelnut	Capsule	Metal Nut	Leather	Pill	Wood	Carpet	Tile	Grid	Cable	Transistor	Toothbrush	Screw	Zipper	Mean
AVID [42]	88.0	86.0	85.0	63.0	58.0	86.0	83.0	70.0	66.0	59.0	64.0	58.0	73.0	66.0	84.0	73.0
AE <sub>2</sub> SIM [6]	88.0	54.0	61.0	54.0	46.0	60.0	83.0	67.0	52.0	69.0	61.0	52.0	74.0	51.0	80.0	63.0
AE <sub>2</sub> L [6]	80.0	88.0	62.0	73.0	44.0	62.0	74.0	50.0	77.0	78.0	56.0	71.0	98.0	69.0	80.0	71.0
AnoGAN [46]	69.0	50.0	58.0	50.0	52.0	62.0	68.0	49.0	51.0	51.0	53.0	67.0	57.0	35.0	59.0	55.0
LSA [1]	86.0	80.0	71.0	67.0	70.0	85.0	75.0	74.0	70.0	54.0	61.0	50.0	89.0	75.0	88.0	73.0
OURS	94.24 $\pm$ 0.10	91.21 $\pm$ 0.13	66.88 $\pm$ 0.23	66.33 $\pm$ 0.10	72.86 $\pm$ 0.86	71.63 $\pm$ 0.11	89.51 $\pm$ 0.63	65.73 $\pm$ 0.37	65.48 $\pm$ 0.12	75.35 $\pm$ 0.60	87.90 $\pm$ 0.10	85.96 $\pm$ 0.12	97.79 $\pm$ 0.05	57.81 $\pm$ 1.12	75.74 $\pm$ 0.13	<b>77.63</b>

## 4.1. Experimental Setup

**Datasets.** We considered 7 datasets for evaluating our method: MNIST, Fashion-MNIST, CIFAR-10, COIL-100, MVTecAD, and 2 medical datasets (Head CT (hemorrhage) and Brain MRI Images for Brain Tumor Detection). We briefly describe each of these datasets:  
**MNIST** [26]: 60k training and 10k test  $28 \times 28$  gray-scale handwritten digit images from 0 to 9. **Fashion-MNIST** [53]: 60k training and 10k test grayscale images of 10 fashion product categories. **CIFAR-10** [25]: 50k training and 10k test  $32 \times 32$  color images in 10 classes. **COIL-100** [33]: 7200  $128 \times 128$  color images of 100 object classes with 72 images of each object in different poses. **MVTecAD** [5]: an industrial dataset with more than 5k high-resolution images in 15 categories of objects and textures. Each category contains both normal and anomalous images with various kinds of defects (used for testing). We downscale all images to the size  $128 \times 128$ , and use zoom data augmentation to create 800 training images for each class. **Head CT (hemorrhage)** [23]: a medical dataset containing 100  $128 \times 128$  normal head CT images and 100 with hemorrhage. **Brain MRI Images for Brain Tumor Detection** [7]: a medical dataset with 98  $256 \times 256$  normal MRI images and 155 with brain tumors.

**Model Configuration and Hyperparameters.** We used the standard U-Net architecture without the batchnorm layers [20] as our base framework which is trained to reconstruct right order images. Moreover, the standard discriminator introduced in DCGAN [38] was used as our next sub-network which was trained to classify the original input and output of the U-Net [27] as real or fake. We used the Adam optimizer [21] for training both networks. The learning rate was initially set to 1e-3 for the U-Net [27] and 2e-4 for the discriminator. We used a learning rate scheduler to multiply the learning rate by 0.8 when the minimum amount of loss did not change for 50 subsequent epochs [17]. Finally, we used the FGSM attack for adversarial robust training of the model. We trained the model until convergence of the loss function with a batch size of 8 for MVTecAD [5] and medical datasets and a batch size of 128 for the rest of the datasets.

**Evaluating Protocols.** The data partitioning used for the training-testing procedures is done similarly to [36] that introduces two protocols. We use Protocol 1 for the COIL-100 [33] dataset that randomly takes one class as the normal data and other classes as anomaly. It uses 80% of all normal

<sup>2</sup>The whole procedure is completely the same as the 4-part puzzle. However, the datum is extended to  $30 \times 30$  and partitioned into 9 parts where 6 parts are permuted and 1 is fully blacked randomly.

samples for the training, and the rest for the test time normal samples. Test time anomalies are sampled from other classes till the number of normal data and anomalous ones be the same. This process is repeated 30 times and the results are averaged. For the medical datasets, we randomly selected 10 normal images and used them along with the anomalous ones for the test data. The rest of the normal images were used for the training. For the MVTecAD [5] dataset, we use the given train and test sets for each class. Zoom augmentation is also performed to create 800 training images for each category of MVTecAD. Protocol 2 is used for all other datasets, which uses the whole training set of just one class as the normal data for training and the whole test set for the test time. We consider 15% of the training data as validation in each dataset. We evaluated the performance using the AUC of the ROC curve which is commonly used for measuring performance in anomaly detection tasks.

## 4.2. Testing Time

To compare execution time of our method with GT [13], we ran the CIFAR-10 experiment on the NVIDIA-GTX1080ti processor with 11 Gigabytes of RAM and with the same batch size. It has been observed that our testing routine has  $4.7 \times$  better execution performance than the GT algorithm.

Table 3: AUROC in % on COIL-100 [33] dataset. Obviously, Puzzle-AE reaches one of the SOTAs.

COIL-100	
Outlier Pursuit [54]	90.8
DPCP [48]	90.0
ALOCC DR [41]	80.9
ALOCC D [41]	68.6
GPND [37]	96.8
OCGAN [36]	<b>99.5</b>
OURS	<b>99.3</b>

Table 4: AUROC in % on real-world medical datasets. We have significant improvement with respect to the other AE-based SOTA methods.

		LSA* [1]	OCGAN* [36]	OURS
Head CT	AUC	$81.67 \pm 0.358$	$51.22 \pm 3.626$	<b><math>86.43 \pm 0.04</math></b>
	FPR	0.81	1.00	<b>0.70</b>
Brain MRI	AUC	$95.61 \pm 1.433$	$91.74 \pm 3.050$	<b><math>96.34 \pm 0.031</math></b>
	FPR	<b>0.40</b>	0.60	0.50

## 4.3. Results

In this section our method’s results are compared with SOTA on the mentioned datasets. We report the mean and

Table 5: Significant better generalization of Puzzle-AE in compression with GT [13].

	GT [13]	OURS
MNIST [26]	<b>98.00</b>	<b>98.00</b>
CIFAR-10 [25]	<b>82.30</b>	72.47
MVTec [5]	67.06*	<b>77.63</b>
Head CT	44.70*	<b>86.43</b>
Brain MRI	82.07*	<b>96.34</b>

variance of our model AUC in the last 20 epochs of training. Other methods’ results are obtained from the main paper or reproduced from their officially released code.

**AUC comparison with SOTA methods:** The AUC results are presented for MNIST [26], Fashion-MNIST [53] and CIFAR-10 [25] in Table. 1, in which Puzzle-AE is compared with the recent SOTAs on these datasets. Table. 2 shows comparison between Puzzle-AE and other SOTA methods on real-world, industrial dataset MVTecAD [5]. Table. 3 shows the results of Puzzle-AE on COIL-100 [33] dataset. In order to show the effectiveness and generalization of the proposed framework, two extra experiments are conducted on 2 different medical datasets, and the results are presented in Table. 4. The results verifies that Puzzle-AE performs significantly better than the competing methods. We also compared our method with a recent self-supervised learning method called GT [13], and the results are shown in Table. 5. Moreover, while GT needs extra expert knowledge to design extra large (72) unambiguous geometric transformations, Puzzle-AE is robust and does not need any expert knowledge. Fig. 9 shows the brittleness of such transformations that become ambiguous with a low amount of noise for competing methods and also shows the robustness of Puzzle-AE in comparison to these methods.

**FPR comparison for high TPR:** As discussed earlier, the two important operating points of ROC curve are when TPR is equal to 99.0% or 99.5%. Fig. 6 shows that Puzzle-AE has significantly lower FPR in those critical points in comparison with LSA [1], while their difference in AUC is not significant. Detailed information is presented in the appendix.

**Model stability:** As shown in the plots provided in the appendix, and in tables 1, 2, 4 the low variances of Puzzle-AE results, indicate the stability of our model in comparison with other methods. Moreover, because of using weight decay, the weights of our model are bounded, which is the consequence of Lipschitz continuity of Puzzle-AE. Proof of Lipschitz continuity is provided in the appendix. Furthermore, Puzzle-AE produces smooth output, and it is shown that [10], being Lipschitz and smooth, the convergence of ADAM optimizer [21] is theoretically provable. This means that we could achieve a highly reliable and stable model at the end of the training phase. This is not the case for other

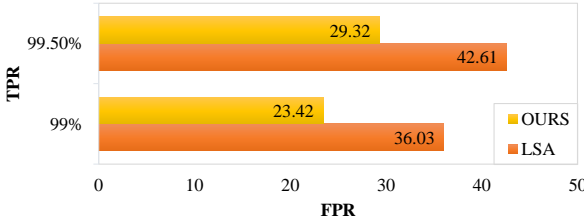


Figure 6: Puzzle-AE has significantly better FPR at TPR equal to 99.5% and 99% in comparison to LSA [1] on the MNIST [26] dataset. The results are averaged over the 10 classes.

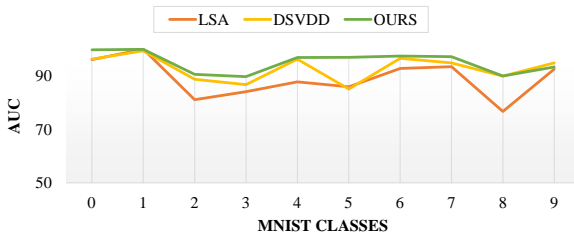


Figure 7: Puzzle-AE has 6% and 3% better performance when trained on the MNIST [26] with 1/12 samples with respect to LSA [1] and DSVDD [40].

methods such as GT [13] and DSVDD [40] as shown in a table in the appendix, where there are large fluctuations of AUC in different epochs of the training process. Because of using unprincipled early stopping methods that usually does not generalize well on unseen datasets, the GT [13] AUC fluctuates nearly by 6% on medical dataset and nearly 30% on MVTecAD [5] dataset while its training accuracy is above 98%. Please see the appendix for more details.

**Effect of training sample size on performance:** Data efficiency, as another important feature that is desired in real-world applications, is shown in Fig. 8 and 7. Traditional AE based approaches usually need a rich dataset to model every complexity in data and obtain good generalization. However, As Fig. 8 illustrates, Puzzle-AE is significantly better than LSA [1] and DAE [49] in terms of data efficiency that is because of its different mean to model abstractions. It is also shown in Fig. 7 that not only Puzzle-AE is significantly better than other SOTA AE based approaches but also, is better than DSVDD [40] which is a one-class method.

**Robustness through attacked normal samples:** Robustness against attacked normal images was examined and the results are reported in Fig. 9. As it is shown, Puzzle-AE is significantly more robust against attacks to normal images with three different values of  $\epsilon$  (0.05, 0.1 and 0.2) in comparison with LSA [1], ARAE [44] and GT [13]. To explain different attacks applied to our method in attack1,

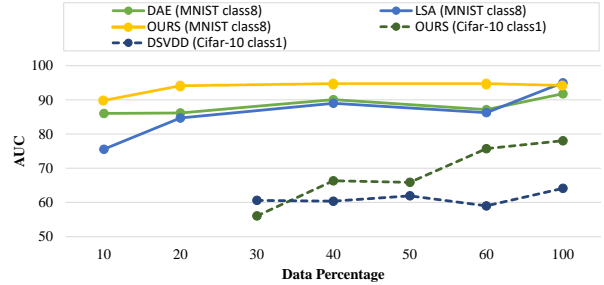


Figure 8: Puzzle-AE is significantly more data efficient than LSA [1] and DAE [49] on the class 8 of the MNIST [26] dataset. Puzzle-AE also performs better than DSVDD [40] in the class car of the CIFAR-10 [25] dataset.

we apply FGSM [51] attack on the normal class before permutation. However, in attack2, we apply FGSM [51] attack on the permuted image. The attacked image is brought back to the original form by using the corresponding inverse permutation. By averaging over all possible permutations, the attacked version of the normal class is obtained.

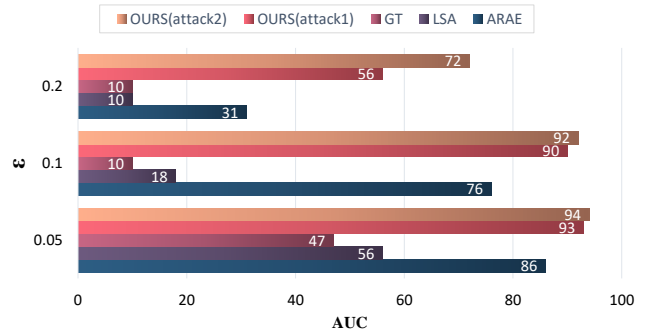


Figure 9: Robustness to adversarial attack on normal data at testing time. The results are shown for three different  $\epsilon$  and the model is trained on class 8 of the MNIST [26] dataset.

**Effect of each component of the proposed method on final performance:** Finally, we conduct experiments to evaluate the effect of every single module or algorithm that has been used in this framework on CIFAR-10 [25] dataset. The experiment and the results are provided in the appendix. As it can be seen, each of these parts has an important role and makes a significant contribution for gaining the best possible performance.

## 5. Ablation

In this section, the effects of several important parameters is examined, as follows, more ablation studies are available in the appendix:

1. **Effect of converting pictures to gray-scale on performance:** It was observed that extracted normal fea-

tures of Puzzle-AE are less sensitive to color for some specific classes of the CIFAR-10 [25] dataset. For example, no significant performance drop observed on the class car of CIFAR-10 [25] when converting the whole dataset to gray-scale. Fig. 5 shows the ability of the proposed model in solving unseen gray-scale puzzled inputs.

2. **Effect of PGD [30], FGSM [51] and random noise on performance:** It was observed that PGD [30] and FGSM [51] have almost similar effects on the performance. However, random noise can not remove shortcuts completely leading to overfitting on some classes of the CIFAR-10 [25], like the car class.

## 6. Conclusion and Future Work

In this study we have tackled two major problems of AEs. Using a U-Net that solves puzzled inputs, not only the quality of reconstructed normal test time inputs is increased but also inability to reconstruct anomalous samples is kept. The experimental results show significant improvements on stability, robustness, data efficiency, generality and FPR at high TPRs on a wide gamut of datasets. In the appendix some deficiencies of our method such as ability to solve some anomalous puzzled inputs is shown. Moreover, a quantitative criterion for selecting min, max or average of the anomaly score could improve the results for future works.

## References

- [1] Davide Abati, Angelo Porrello, Simone Calderara, and Rita Cucchiara. Latent space autoregression for novelty detection. In *Proceedings of the IEEE Conference on Computer Vision and Pattern Recognition*, pages 481–490, 2019. 2, 6, 7, 8, 13, 14, 15
- [2] Samet Akcay, Amir Atapour-Abarghouei, and Toby P Breckon. Gandomaly: Semi-supervised anomaly detection via adversarial training. In *Asian Conference on Computer Vision*, pages 622–637. Springer, 2018. 3, 4
- [3] Vijay Badrinarayanan, Alex Kendall, and Roberto Cipolla. Segnet: A deep convolutional encoder-decoder architecture for image segmentation. *IEEE transactions on pattern analysis and machine intelligence*, 39(12):2481–2495, 2017. 2
- [4] Christoph Baur, Benedikt Wiestler, Shadi Albarqouni, and Nassir Navab. Deep autoencoding models for unsupervised anomaly segmentation in brain mr images. In *International MICCAI Brainlesion Workshop*, pages 161–169. Springer, 2018. 1
- [5] Paul Bergmann, Michael Fauser, David Sattlegger, and Carsten Steger. Mvtac ad—a comprehensive real-world dataset for unsupervised anomaly detection. In *Proceedings of the IEEE Conference on Computer Vision and Pattern Recognition*, pages 9592–9600, 2019. 2, 5, 6, 7, 8, 12, 13
- [6] Paul Bergmann, Sindy Löwe, Michael Fauser, David Sattlegger, and Carsten Steger. Improving unsupervised defect segmentation by applying structural similarity to autoencoders. In *International Joint Conference on Computer Vision, Imaging and Computer Graphics Theory and Applications (VISIGRAPP)*, 2019. 6
- [7] Navoneel Chakrabarty. Brain mri images for brain tumor detection. <https://www.kaggle.com/navoneel/brain-mri-images-for-brain-tumor-detection>, 2019. 2, 6
- [8] Raghavendra Chalapathy and Sanjay Chawla. Deep learning for anomaly detection: A survey. *arXiv preprint arXiv:1901.03407*, 2019. 1
- [9] Xiaoran Chen and Ender Konukoglu. Unsupervised detection of lesions in brain mri using constrained adversarial auto-encoders. *arXiv preprint arXiv:1806.04972*, 2018. 1, 4
- [10] Xiangyi Chen, Sijia Liu, Ruoyu Sun, and Mingyi Hong. On the convergence of a class of adam-type algorithms for non-convex optimization. *arXiv preprint arXiv:1808.02941*, 2018. 7
- [11] Yunqiang Chen, Xiang Sean Zhou, and Thomas S Huang. One-class svm for learning in image retrieval. In *Proceedings 2001 International Conference on Image Processing (Cat. No. 01CH37205)*, volume 1, pages 34–37. IEEE, 2001. 6
- [12] Jia Deng, Wei Dong, Richard Socher, Li-Jia Li, Kai Li, and Li Fei-Fei. Imagenet: A large-scale hierarchical image database. In *2009 IEEE conference on computer vision and pattern recognition*, pages 248–255. Ieee, 2009. 2
- [13] Izhak Golan and Ran El-Yaniv. Deep anomaly detection using geometric transformations. In *Advances in Neural Information Processing Systems*, pages 9758–9769, 2018. 2, 3, 7, 8, 12, 13
- [14] Dong Gong, Lingqiao Liu, Vuong Le, Budhaditya Saha, Moussa Reda Mansour, Svetha Venkatesh, and Anton van den Hengel. Memorizing normality to detect anomaly: Memory-augmented deep autoencoder for unsupervised anomaly detection. In *Proceedings of the IEEE International Conference on Computer Vision*, pages 1705–1714, 2019. 1, 3, 13, 15
- [15] Ian Goodfellow. Nips 2016 tutorial: Generative adversarial networks. *arXiv preprint arXiv:1701.00160*, 2016. 2
- [16] Ian J Goodfellow, Jonathon Shlens, and Christian Szegedy. Explaining and harnessing adversarial examples. *arXiv preprint arXiv:1412.6572*, 2014. 3, 4
- [17] Priya Goyal, Piotr Dollár, Ross Girshick, Pieter Noordhuis, Lukasz Wesolowski, Aapo Kyrola, Andrew Tulloch, Yangqing Jia, and Kaiming He. Accurate, large mini-batch sgd: Training imagenet in 1 hour. *arXiv preprint arXiv:1706.02677*, 2017. 6
- [18] Dan Hendrycks, Mantas Mazeika, Saurav Kadavath, and Dawn Song. Using self-supervised learning can improve model robustness and uncertainty. In *Advances in Neural Information Processing Systems*, pages 15663–15674, 2019. 2
- [19] Andrew Ilyas, Shibani Santurkar, Dimitris Tsipras, Logan Engstrom, Brandon Tran, and Aleksander Madry. Adversarial examples are not bugs, they are features. In *Advances*

*in Neural Information Processing Systems*, pages 125–136, 2019. 2

[20] Sergey Ioffe and Christian Szegedy. Batch normalization: Accelerating deep network training by reducing internal covariate shift. *arXiv preprint arXiv:1502.03167*, 2015. 6

[21] Diederik P Kingma and Jimmy Ba. Adam: A method for stochastic optimization. *arXiv preprint arXiv:1412.6980*, 2014. 6, 7

[22] Diederik P Kingma and Max Welling. Auto-encoding variational bayes. *arXiv preprint arXiv:1312.6114*, 2013. 3

[23] Felipe Kitamura. Head ct - hemorrhage. <https://www.kaggle.com/felipekitamura/head-ct-hemorrhage>, 2018. 2, 6

[24] Naveen Kodali, Jacob Abernethy, James Hays, and Zsolt Kira. On convergence and stability of gans. *arXiv preprint arXiv:1705.07215*, 2017. 2

[25] Alex Krizhevsky, Vinod Nair, and Geoffrey Hinton. Cifar-10 (canadian institute for advanced research). 2009. 2, 5, 6, 7, 8, 9, 13, 14, 15

[26] Yann LeCun, Corinna Cortes, and CJ Burges. Mnist handwritten digit database. 2010. 6, 7, 8, 13, 14

[27] Xiaomeng Li, Hao Chen, Xiaojuan Qi, Qi Dou, Chi-Wing Fu, and Pheng-Ann Heng. H-denseunet: hybrid densely connected unet for liver and tumor segmentation from ct volumes. *IEEE transactions on medical imaging*, 37(12):2663–2674, 2018. 4, 6

[28] Xiaoyan Li, Iluju Kiringa, Tet Yeap, Xiaodan Zhu, and Yifeng Li. Exploring deep anomaly detection methods based on capsule net. In *ICML 2019 Workshop on Uncertainty and Robustness in Deep Learning, At Long Beach*, 2019. 6

[29] Geert Litjens, Thijs Kooi, Babak Ehteshami Bejnordi, Arnaud Arindra Adiyoso Setio, Francesco Ciompi, Mohsen Ghafoorian, Jeroen Awm Van Der Laak, Bram Van Ginneken, and Clara I Sánchez. A survey on deep learning in medical image analysis. *Medical image analysis*, 42:60–88, 2017. 2, 4

[30] Aleksander Madry, Aleksandar Makelov, Ludwig Schmidt, Dimitris Tsipras, and Adrian Vladu. Towards deep learning models resistant to adversarial attacks. *arXiv preprint arXiv:1706.06083*, 2017. 2, 4, 9

[31] Arjovsky Martin and B Lon. Towards principled methods for training generative adversarial networks. In *NIPS 2016 Workshop on Adversarial Training. In review for ICLR*, volume 2016, 2017. 2

[32] Eric Nalisnick, Akihiro Matsukawa, Yee Whye Teh, Dilan Gorur, and Balaji Lakshminarayanan. Do deep generative models know what they don’t know? *arXiv preprint arXiv:1810.09136*, 2018. 2

[33] Sameer A. Nene, Shree K. Nayar, and Hiroshi Murase. object image library (coil-100. Technical report, 1996. 6, 7, 13

[34] Mehdi Noroozi and Paolo Favaro. Unsupervised learning of visual representations by solving jigsaw puzzles. In *European Conference on Computer Vision*, pages 69–84. Springer, 2016. 2, 4

[35] Aaron van den Oord, Yazhe Li, and Oriol Vinyals. Representation learning with contrastive predictive coding. *arXiv preprint arXiv:1807.03748*, 2018. 2

[36] Pramuditha Perera, Ramesh Nallapati, and Bing Xiang. Ocgan: One-class novelty detection using gans with constrained latent representations. In *Proceedings of the IEEE Conference on Computer Vision and Pattern Recognition*, pages 2898–2906, 2019. 3, 6, 7

[37] Stanislav Pidhorskyi, Ranya Almohsen, and Gianfranco Doretto. Generative probabilistic novelty detection with adversarial autoencoders. In *Advances in neural information processing systems*, pages 6822–6833, 2018. 7

[38] Alec Radford, Luke Metz, and Soumith Chintala. Unsupervised representation learning with deep convolutional generative adversarial networks. *arXiv preprint arXiv:1511.06434*, 2015. 6

[39] Olaf Ronneberger, Philipp Fischer, and Thomas Brox. U-net: Convolutional networks for biomedical image segmentation. In *International Conference on Medical image computing and computer-assisted intervention*, pages 234–241. Springer, 2015. 2

[40] Lukas Ruff, Robert Vandermeulen, Nico Goernitz, Lucas Deecke, Shoaib Ahmed Siddiqui, Alexander Binder, Emmanuel Müller, and Marius Kloft. Deep one-class classification. In *International conference on machine learning*, pages 4393–4402, 2018. 2, 3, 6, 8, 12, 13, 14

[41] Mohammad Sabokrou, Mohammad Khalooei, Mahmood Fathy, and Ehsan Adeli. Adversarially learned one-class classifier for novelty detection. In *Proceedings of the IEEE Conference on Computer Vision and Pattern Recognition*, pages 3379–3388, 2018. 2, 7

[42] Mohammad Sabokrou, Masoud Pourreza, Mohsen Fayyaz, Rahim Entezari, Mahmood Fathy, Jürgen Gall, and Ehsan Adeli. Avid: Adversarial visual irregularity detection. In *Asian Conference on Computer Vision*, pages 488–505. Springer, 2018. 4, 6

[43] Mayu Sakurada and Takehisa Yairi. Anomaly detection using autoencoders with nonlinear dimensionality reduction. In *Proceedings of the MLSDA 2014 2nd Workshop on Machine Learning for Sensory Data Analysis*, pages 4–11, 2014. 2

[44] Mohammadreza Salehi, Atrin Arya, Barbad Pajoum, Mohammad Otoofi, Amirreza Shaeiri, Mohammad Hossein Rohban, and Hamid R Rabiee. Arae: Adversarially robust training of autoencoders improves novelty detection. *arXiv preprint arXiv:2003.05669*, 2020. 4, 6, 8

[45] Tim Salimans, Ian Goodfellow, Wojciech Zaremba, Vicki Cheung, Alec Radford, and Xi Chen. Improved techniques for training gans. In *Advances in neural information processing systems*, pages 2234–2242, 2016. 2

[46] Thomas Schlegl, Philipp Seeböck, Sebastian M Waldstein, Ursula Schmidt-Erfurth, and Georg Langs. Unsupervised anomaly detection with generative adversarial networks to guide marker discovery. In *International conference on information processing in medical imaging*, pages 146–157. Springer, 2017. 3, 6

[47] Ilya Tolstikhin, Olivier Bousquet, Sylvain Gelly, and Bernhard Schoelkopf. Wasserstein auto-encoders. *arXiv preprint arXiv:1711.01558*, 2017. 4

[48] Manolis C Tsakiris and René Vidal. Dual principal component pursuit. *The Journal of Machine Learning Research*, 19(1):684–732, 2018. 7

[49] Pascal Vincent, Hugo Larochelle, Yoshua Bengio, and Pierre-Antoine Manzagol. Extracting and composing robust features with denoising autoencoders. In *Proceedings of the 25th international conference on Machine learning*, pages 1096–1103, 2008. 8

[50] Xiaosong Wang, Yifan Peng, Le Lu, Zhiyong Lu, Mohammad Bagheri, and Ronald M Summers. Chestx-ray8: Hospital-scale chest x-ray database and benchmarks on weakly-supervised classification and localization of common thorax diseases. In *Proceedings of the IEEE conference on computer vision and pattern recognition*, pages 2097–2106, 2017. 4

[51] Eric Wong, Leslie Rice, and J Zico Kolter. Fast is better than free: Revisiting adversarial training. *arXiv preprint arXiv:2001.03994*, 2020. 4, 8, 9

[52] Zhirong Wu, Yuanjun Xiong, Stella X Yu, and Dahua Lin. Unsupervised feature learning via non-parametric instance discrimination. In *Proceedings of the IEEE Conference on Computer Vision and Pattern Recognition*, pages 3733–3742, 2018. 2

[53] Han Xiao, Kashif Rasul, and Roland Vollgraf. Fashion-mnist: a novel image dataset for benchmarking machine learning algorithms. *arXiv preprint arXiv:1708.07747*, 2017. 6, 7, 13

[54] Huan Xu, Constantine Caramanis, and Sujay Sanghavi. Robust pca via outlier pursuit. In *Advances in Neural Information Processing Systems*, pages 2496–2504, 2010. 7

[55] Shuangfei Zhai, Yu Cheng, Weining Lu, and Zhongfei Zhang. Deep structured energy based models for anomaly detection. *arXiv preprint arXiv:1605.07717*, 2016. 6

[56] Richard Zhang, Phillip Isola, and Alexei A Efros. Split-brain autoencoders: Unsupervised learning by cross-channel prediction. In *Proceedings of the IEEE Conference on Computer Vision and Pattern Recognition*, pages 1058–1067, 2017. 2

[57] Bo Zong, Qi Song, Martin Renqiang Min, Wei Cheng, Cristian Lumezanu, Daeki Cho, and Haifeng Chen. Deep autoencoding gaussian mixture model for unsupervised anomaly detection. 2018. 6

# Appendix

## A. Proof of Lipschitz Continuity of Puzzle-AE

Let  $w$  denotes the weights of our model and let  $\mathcal{L}$  be the total loss. Because of using weight decay, the main objective of the training procedure is defined as:

$$\min_w \mathcal{L} + c\|w\|_{\mathcal{F}}^2 \quad (8)$$

where  $\|\cdot\|_{\mathcal{F}}$  denotes the Frobenius norm and  $c$  is a constant. This is equivalent to:

$$\min_w \mathcal{L} \text{ s.t. } \|w\|_{\mathcal{F}}^2 \leq M \quad (9)$$

which means that the model weights are bounded by some constant  $M$ . Also, because all of the activation functions are smooth, they have limited derivative values. This results in having limited upper bound for the whole network.

## B. Model Stability

We provide additional results showing that Puzzle-AE has more stability in comparison with other methods. Figures 10, 12, 11, 13 are the min, max, and average AUC plots with respect to training epochs. These plots show that we could achieve a highly reliable and stable model at the end of the training phase, as opposed to other methods such as GT[13] and DSVDD[40] as shown in Table. 6. The results show that these methods have large fluctuations of AUC in different epochs of their training process.

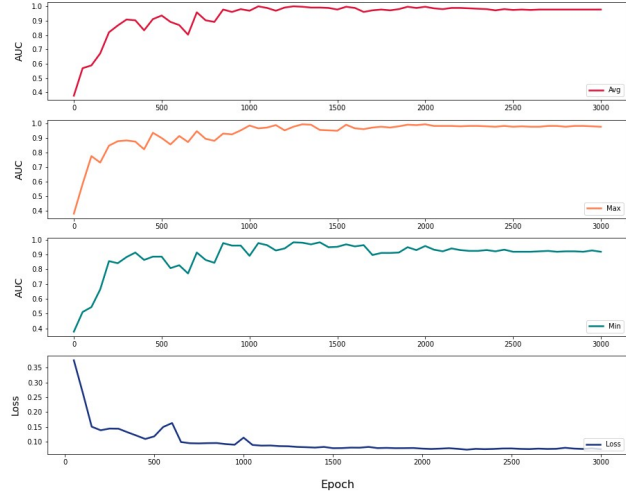


Figure 10: Min, max and avg AUC Plots with respect to training epochs are shown for the class toothbrush of the MVTecAD [5] dataset. As it is shown, training procedure continues till the convergence of all of the AUC plots and also loss value.

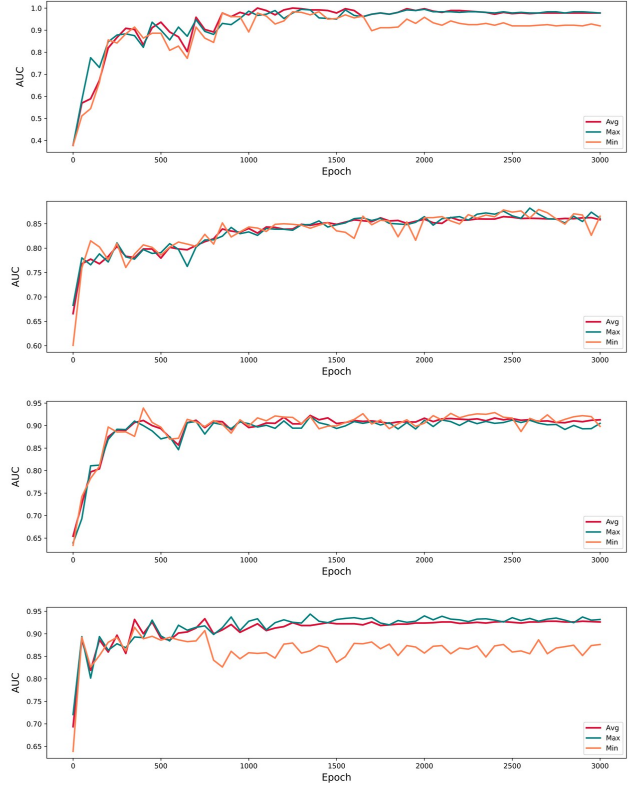


Figure 11: Min, max and avg AUC Plots with respect to training epochs are shown for the classes toothbrush, transistor, hazelnut and bottle of the MVTecAD [5] dataset.

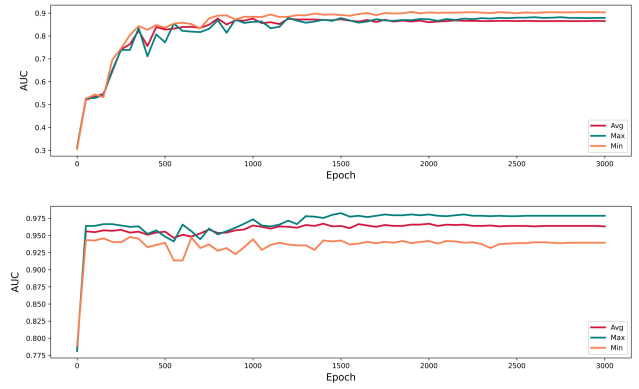


Figure 12: Min, max and avg AUC Plots with respect to training epochs are shown for each medical dataset.

Table 6: Up - GT [13] AUC fluctuations during training procedure on head ct medical and the capsule class of MVTecAD [5] dataset. Bottom - DSVDD [40] AUC fluctuations during last 16 epochs of training procedure on the class car of CIFAR-10 [25] dataset.

Method	Dataset	0	1	2	3	4	5	6	7	8	9	10	11	12	13	14	15	16	
GT [13]	Head CT	AUC	56.52	53.68	54.26	69.29	67.10	69.87	77.48	79.03	<b>76.45</b>	77.48	79.55	80.06	<b>81.23</b>	80.90	77.68	79.23	<b>75.03</b>
		Train ACC	14.59	34.45	43.41	55.84	71.17	90.08	98.88	99.92	<b>99.98</b>	100	100	100	<b>100</b>	100	99.93	99.60	<b>98.14</b>
	MVTec (Capsule)	AUC	<b>45.95</b>	67.41	71.20	74.11	<b>77.46</b>	60.75	64.10	73.00	73.00	62.82	62.50	66.29	69.49	<b>60.63</b>	66.85	73.35	68.93
		Train ACC	<b>98.89</b>	99.50	100	100	<b>100</b>	99.99	100	100	100	100	100	99.55	100	<b>98.49</b>	100	100	100
DSVDD [40]	Cifar-10 (Car)	AUC	56.21	<b>51.83</b>	53.74	54.50	57.57	59.86	60.23	<b>60.60</b>	59.81	56.37	57.72	55.82	58.40	54.04	54.97	55.25	56.22
		Train loss	0.577	<b>0.477</b>	0.387	0.332	0.328	0.314	0.306	<b>0.300</b>	0.288	0.282	0.267	0.259	0.251	0.242	0.229	0.218	0.211

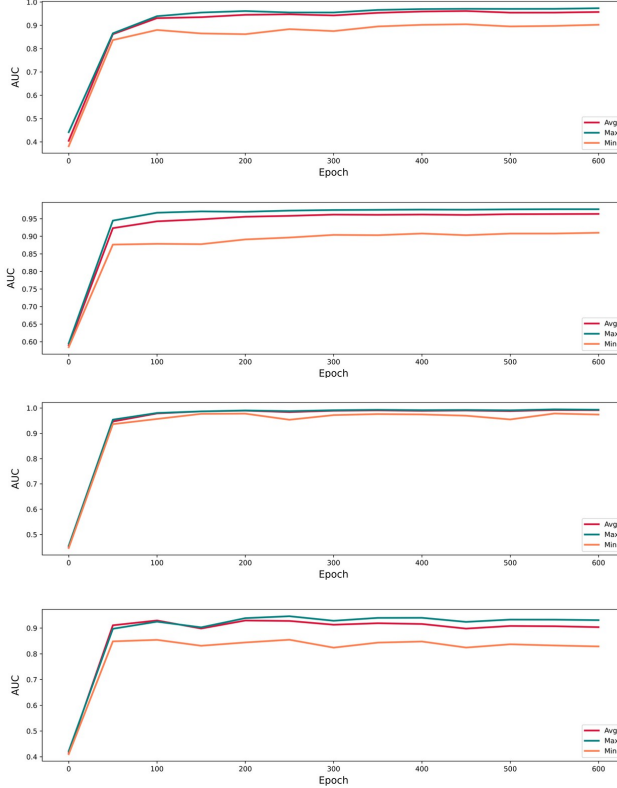


Figure 13: Min, max and avg AUC Plots with respect to training epochs are shown for the classes 2, 4, 6 and 8 of the MNIST [26] dataset.

### C. Effect of training sample size on performance

Table. 7 provides more detail comparing data efficiency of Puzzle-AE with other methods such as LSA [1] and DSVDD [40]. It was observed that by dividing the number of training samples by 12 in MNIST[26] dataset, the performance drop of Puzzle-AE is about 3.1 percent.

### D. FPR comparison for high TPR

We provide additional results in Table. 8 comparing FPR in Puzzle-AE and LSA [1] at TPR equal to 99.5% and 99% on all

classes of the MNIST [26] dataset. The results show that Puzzle-AE has significantly better FPR at high values of TPR.

### E. Effect of Each Component of the Puzzle-AE on Final Performance

Table. 9 shows the effect of each single module or algorithm that has been used in this framework on CIFAR-10[25] dataset. The results are shown for puzzle-solving AE (PAE), puzzle-solving and colorization (CPAE), and also CPAE combined with adversarial training (CPAE-G (GAN)). The results show that each of these parts has an important role for gaining the best possible performance.

### F. Effect of simple architectural changes on performance

It was observed that by halving the number of filters in each layer, performance does not drop significantly, specifically for MNIST[26], Fashion-MNIST[53] and COIL-100 [33] datasets. Hence, if testing time or testing memory is important for a simple real world application, it can be halved without any significant performance drop.

### G. Visualization of Puzzle-AE on Different Datasets

We give additional qualitative results from different datasets in Fig. 14, 15, and 16. Fig. 17 shows the reconstruction of Puzzle-AE trained on class car of the CIFAR-10[25] dataset for some anomalous inputs. It can be seen that the model has good reconstruction for anomalous inputs which have main features similar to the normal class. Fig. 18 compares the reconstruction of our model with LSA [1] and MemAE [14] for both normal and anomalous inputs.

Table 7: Puzzle-AE has 6% and 3% better performances when trained on the MNIST [26] with 1/12 samples with respect to LSA [1] and DSVDD [40].

Method	0	1	2	3	4	5	6	7	8	9	mean
LSA* [1]	95.93 $\pm$ 0.087	99.82 $\pm$ 0.005	80.95 $\pm$ 0.119	83.95 $\pm$ 0.090	87.59 $\pm$ 0.113	85.81 $\pm$ 0.072	92.61 $\pm$ 0.059	93.31 $\pm$ 0.074	76.56 $\pm$ 0.328	92.40 $\pm$ 0.075	88.89
DSVDD* [40]	96.10 $\pm$ 0.057	99.17 $\pm$ 0.006	88.62 $\pm$ 0.146	86.60 $\pm$ 0.252	95.09 $\pm$ 0.024	84.93 $\pm$ 0.091	96.40 $\pm$ 0.058	94.68 $\pm$ 0.036	89.76 $\pm$ 0.121	94.72 $\pm$ 0.044	92.61
OURS	99.54 $\pm$ 0.044	99.73 $\pm$ 0.034	90.41 $\pm$ 0.593	89.59 $\pm$ 1.056	95.71 $\pm$ 0.306	96.79 $\pm$ 0.504	97.23 $\pm$ 0.310	96.98 $\pm$ 0.189	89.81 $\pm$ 0.676	93.17 $\pm$ 0.592	<b>94.90</b>

Table 8: Puzzle-AE has significantly better TPR at FPR equal to 99.5% and 99.0% than LSA [1] on the MNIST [26] dataset for 10 class average.

TPR	Method	0	1	2	3	4	5	6	7	8	9	Mean
99%	LSA* [1]	0.0765	0.0088	0.7238	0.4119	0.6365	0.3274	0.1190	0.4591	0.5975	0.2428	0.3603
	OURS	0.0480	0.0053	0.3295	0.2079	0.3157	0.1939	0.1086	0.2451	0.7156	0.1724	<b>0.2342</b>
99.5%	LSA* [1]	0.0980	0.0123	0.8178	0.4871	0.7210	0.3924	0.1587	0.5447	0.7146	0.3142	0.4261
	OURS	0.0694	0.0088	0.4079	0.2545	0.4287	0.3262	0.1441	0.2977	0.7895	0.2061	<b>0.2932</b>



Figure 14: Visualization of the proposed method on CIFAR-10 [25] dataset. First row is the original input, second row is the puzzled input mingled by colorization task and the third row is the unpuzzled output.

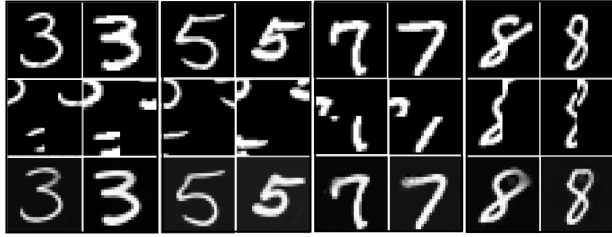


Figure 15: Visualization of the proposed method on MNIST [26] dataset. First row is the original input, second row is the puzzled input mingled by inpainting task and the third row is the unpuzzled output.

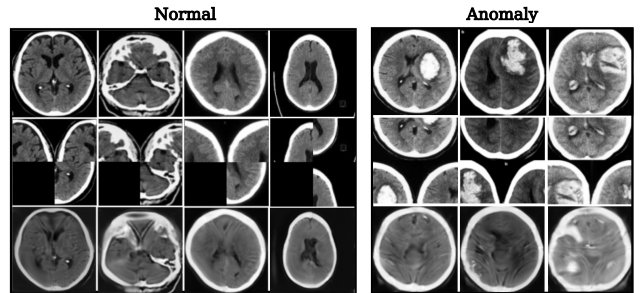


Figure 16: Visualization of the proposed method on Head CT dataset. First row is the original input, second row is the puzzled input mingled by the inpainting task, and the third row is the unpuzzled output solved by the model.

Table 9: Effect of each component or algorithm is illustrated separately. As it is shown, CPAE-G has the best results on sample dataset CIFAR-10 [25].

		0	1	2	3	4	5	6	7	8	9	mean
MIN	puzzle AE (PAE)	76.32	69.69	68.70	54.08	75.30	62.91	72.72	69.61	80.87	64.88	69.51
	colorization + puzzle (CPAE)	79.51	69.77	68.51	54.75	72.56	63.24	67.86	68.30	82.09	65.57	69.22
	colorization + puzzle + GAN (CPAE-G)	79.42	73.00	69.48	53.00	73.98	65.13	68.98	70.65	83.28	66.73	70.37
MAX	puzzle AE (PAE)	76.29	69.07	68.19	52.14	75.84	60.84	73.66	68.61	78.26	66.20	68.91
	colorization + puzzle (CPAE)	78.87	76.56	67.97	54.33	74.69	62.32	75.72	71.59	81.06	70.92	71.40
	colorization + puzzle + GAN (CPAE-G)	77.21	77.31	69.3	54.10	74.76	64.10	76.02	70.42	81.04	66.91	71.12
AVG	puzzle AE (PAE)	76.59	68.84	68.54	53.00	76.00	61.8	73.32	68.87	79.54	66.12	69.26
	colorization + puzzle (CPAE)	79.72	75.86	68.56	54.74	74.87	64.21	74.02	72.97	82.64	70.62	71.82
	colorization + puzzle + GAN (CPAE-G)	78.93	78.05	69.95	54.88	75.46	66.04	74.76	73.30	83.34	69.96	<b>72.47</b>

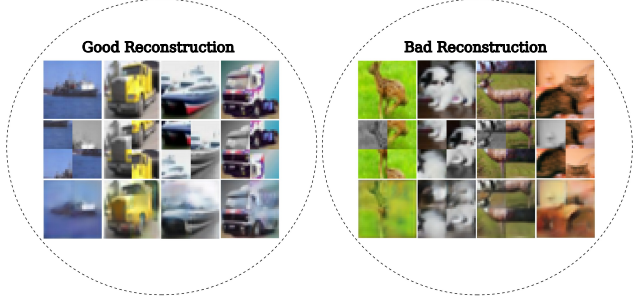


Figure 17: Anomalous reconstruction of the model trained on the class car of the CIFAR-10 [25] dataset. Good reconstruction occurs in classes with high similarity in main features such as truck and ship.

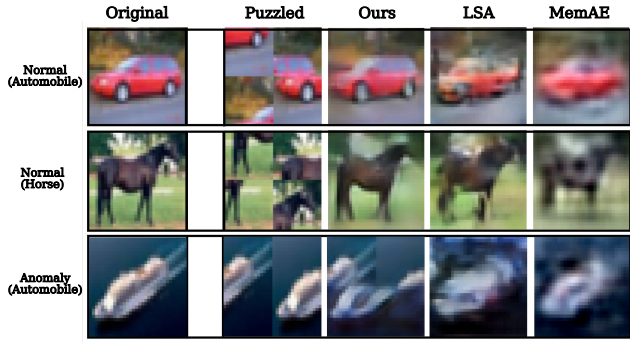


Figure 18: Reconstruction of LSA [1], MemAE [14] and Puzzle-AE on normal and anomalous test inputs. Models are trained on the given class. Last row shows the reconstruction of an anomalous input when the models are trained on class Automobile as the normal class. Obviously our model produces significantly better normal outputs while destroys the anomalous ones.